International Journal of Geosciences, 2025, 16(1), 31-60
https://www.scirp.org/journal/ijg
ISSN Online: 2156-8367
ISSN Print: 2156-8359

Geomorphometric Analysis of the Kshetrapal Landslide in Chamoli, Uttarakhand, India Using the White Box Tool (WBT) and QGIS by Comparing Various DEMs Obtained from UAV and TLS

Ashok Anand

Geomatics Engineering Group, Department of Civil Engineering, Indian Institute of Technology Roorkee, Uttarakhand, India
Email: a_anand@ce.iitr.ac.in

How to cite this paper: Anand, A. (2025) Geomorphometric Analysis of the Kshetrapal Landslide in Chamoli, Uttarakhand, India Using the White Box Tool (WBT) and QGIS by Comparing Various DEMs Obtained from UAV and TLS. *International Journal of Geosciences*, **16**, 31-60.
https://doi.org/10.4236/ijg.2025.161003

Received: November 14, 2024
Accepted: January 19, 2025
Published: January 22, 2025

Abstract

Utilizing multispectral satellite data and digital elevation models (DEMs) has emerged as the primary approach for cartographically representing landforms. By using high-resolution satellite photos that capture spatial, temporal, spectral, and radiometric data, one may get a fresh comprehension of the geomorphology of a particular area by recognizing its landforms. In addition, a synergistic method is used by using data produced from digital elevation models (DEMs) such as Slope, Aspect, Hillshade, Curvature, Contour Patterns, and 3-D Flythrough Visuals. The increasing use of UAV (drone) technology for obtaining high-resolution digital images and elevation models has become an essential element in developing complete topographic models in landslide scars that are very unstable and prone to erosion. Comparison (differences in values) of seven (7) different DEMs between two algorithms used, *i.e.*, QGIS and White Box Tool (WBT), were successfully attempted in the present research. The TLS, UAV and Satellite data of the study area—Kshetrapal Landslide, Chamoli (District), Uttarakhand (State), India was subjected to two different algorithms (QGIS and WBT) to evaluate and differentiate seven different DEMs (CARTOSAT, ASTER, SRTM, Alos 3D, TanDEM, MERIT, and FabDEM/FATHOM) taking into consideration various parameters viz. Aspect, Hillshade, Slope, Mean Curvature, Plan Curvature, Profile Curvature and Total Curvature. The different values of aforesaid parameters of various DEMs evaluated (using algorithms QIGS and WBT) reveal that only three parameters, *i.e.*, Aspect, Hillshade, and Slope, show results. In contrast, the remaining ones do not show any meaningful results, and therefore, the comparison was possible only with regard to these three parameters. The comparison is drawn by comparing minimum, maximum, and elevation values (by subtracting WBT values from QGIS values) regarding Aspect, Hillshade, and Slope, arranging the differences in values as per their importance. (Increasing or decreasing order), assigning merit scores individually, and then cumulatively, and ascertaining the order of application suitability of various Dems, which stand in the order of (CARTOSAT, ASTER, SRTM, Alos 3D, TanDEM, and MERIT, and FabDEM/FATHOM).

Keywords

Landslide, Morphometric Analysis, Digital Elevation Models (DEMs), TLS, UAV (Drone), QGIS, WBT

1. Introduction

In the past ten years, there has been a rise in the utilization of remote sensing technology to track and map avalanches. The spatial accuracy of satellite imaging has greatly improved, especially with the implementation of laser imaging, both in aerial and lowland applications [1]. It is necessary to enhance the comprehension of landslide processes, ascertain the factors that initiate avalanches, devise techniques for predicting the likelihood of landslides, maintain past documentation of landslides, and establish adaptable and dependable monitoring tools [2]. Single-point systems such as total stations, the GNSS, and crack monitoring equipment are commonly employed in the conventional methods of landslip detection [3]. These results suggest that these models are not proficient in accurately representing the general strain characteristics of large-scale landslides. However, they are highly efficient for tracking the movement of avalanches at local levels [4]. By recording the relative or absolute movement of tracking points, these devices or gear offer a precise representation of the advancement of the landslide. Although such typical monitoring methods are highly precise, their monitoring length is limited by the scattered nature of the tools and the number of units used for monitoring [5]. Due to recent advancements in satellite imagery, it has now become possible to collect geographical information on an extensive level. This greatly facilitates the identification and monitoring of landslides. A platform-based remote sensing technique that might be cited as an example is the utilization of high-resolution satellites in space along with Synthetic Aperture Radar (SAR). Another instance involves the utilization of aerial light detection and ranging (LiDAR) and photogrammetry through unmanned aerial vehicles (UAV), which are two interconnected innovations [6]. Additionally, there is a third category of devices known as ground-based devices, which encompass Ground-Based Interferometric SAR (GB-SAR) and Terrestrial Laser Scanning (TLS). Research investigating the vulnerability of landslides, assessing distortion, and detecting massive landslide hazards have demonstrated fruitful uses for space-borne technologies

[7]. An imagery-processing approach is employed to track disasters in detail by combining the usage of UAVs, computer vision, and image correlation algorithms. However, before discussing this workflow, it first examined the remote sensor techniques utilized for monitoring landslides, starting from low-resolution methods and progressing to higher resolutions [8]. Landslide studies have utilized a diverse array of remote sensing techniques, including optical detectors, heat sensors, LiDAR, and microwave detectors, operating at various time and spatial scales and from space-borne, airborne, or ground-based platforms [9]. Earth-observing techniques are valuable for generating precise and comprehensive collections of photographs, orthophotos, and DEMs over many periods. These products can offer valuable information on the dynamics and characteristics of the flow, like the velocity of flow, the growth of landslides, and the buildup of material at the bottom area or receding slopes [10]. Furthermore, these novel methodologies enable the computation of the quantity of material that has been both deposited and eroded by the landslide, as well as the tracing of the alterations in the topography [11]. Laser imaging techniques, like aerial LiDAR and TLS, can provide precise and comprehensive 3D data on the ground surface [12]. TLS is a method that utilizes lasers from a fixed location to accurately determine the position and dimensions of objects in three-dimensional space. The detection of landslide motions can be achieved by analyzing consecutive scans [13]. Landslide vulnerability evaluations in the avalanche-prone regions of Uttarakhand state, India, were examined using three Machine Learning (ML) algorithms. The success rate of these strategies has been compared using different statistical index-based techniques. The evaluation of findings indicates that the stated landslide models showed strong performance in assessing susceptibility to landslides [14]. Aerial photogrammetry and topographical Lidar techniques are used to create high-resolution DEMs. It utilized the Rapid Mass Movement Simulation (RAMMS) software to assess how sensitive it is to the origin and spatial resolution of the DEMs when modeling a massive and intricate snow landslide. It was discovered that RAMMS demonstrated excellent performance under difficult situations while utilizing the high-resolution 2 m lidar DSM. Specifically, 99 % of the modeled debris volume was found within the designated debris area [15]. The two ongoing landslides in Pakistan, Nara and Nokot, were characterized and evaluated for their geomorphic alterations using UAV images and topographic data [16]. The use of TLS point clouds has been found to result in higher density and more suitability for improving the preciseness of the monitoring process. The results were verified using data obtained from the GNSS. TLS and UAV were used for analyzing the structural integrity of rock slopes [17]. Research done in [18] examined the ongoing and regular tracking of landslide movements utilizing information from GNSS, a wire extensometer, UAV photogrammetry, and hydro-meteorological sensing (groundwater table, precipitation). The findings of another study indicated that the behavior of the Urbas landslide varies throughout different sections of the landslide region, influenced by the specific geological and hydrogeological characteristics

of each location [18]. A study was conducted to evaluate the suitability of using several types of remote sensing data, including satellite imagery, UAVs, and TLS, in combination with process-oriented modeling [19].

2. Research Contribution

In this research, the Kshetrapal landslide in Chamoli, Himalayas, was effectively assessed using UAV equipped with high-resolution camera. The UAV quickly mapped the extent of the landslide and detected potential dangers such as unstable slopes. TLS allowed for accurate measurements at ground level, facilitating the creation of detailed 3D terrain model and investigation of surface changes after a landslide. Using this comprehensive method enhanced comprehension of the mechanisms behind landslides, thereby assisting in the evaluation of potential risks, the development of emergency plans, and the formulation of sustainable measures to minimize the impact of such events in the vulnerable Himalayan ecosystem. UAV and TLS technologies are essential in strengthening resilience against future natural disasters in high-risk zones by improving the monitoring and management of areas prone to landslides.

The following figures (**Figure 1** to **Figure 15**) show various equipment and relevant details while collecting data using UAV and TLS as indicated in the figure key below.

Figure 1. UAV (SNAP-M) (Drone).

Figure 2. UAV flight planning of the site for collecting data.

Figure 3. TLS (FARO S350+).

Figure 4. Showing TLS scanning the landslide.

Figure 5. Showing shapefile of landslide area.

Figure 6. Showing mosaic landslide area.

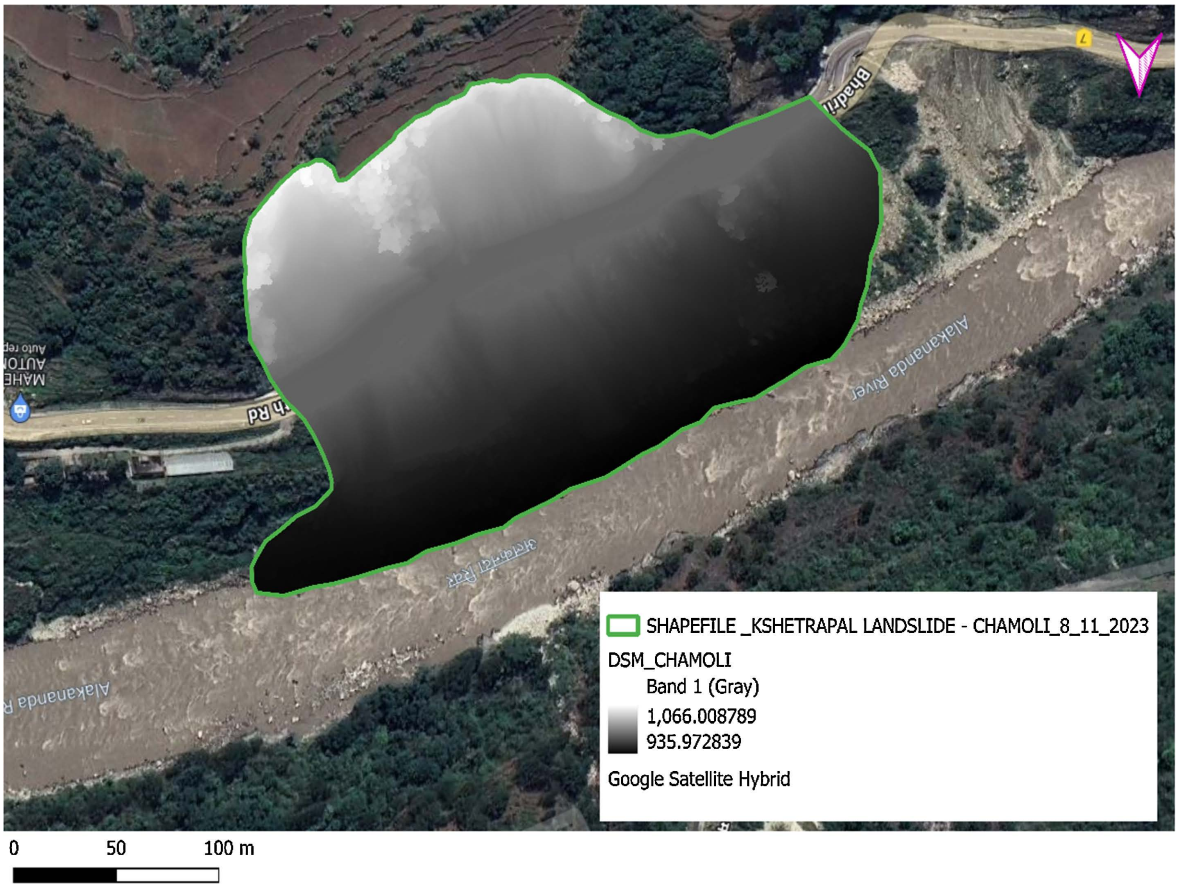

Figure 7. Showing Digital Surface Model (DSM) of landslide area.

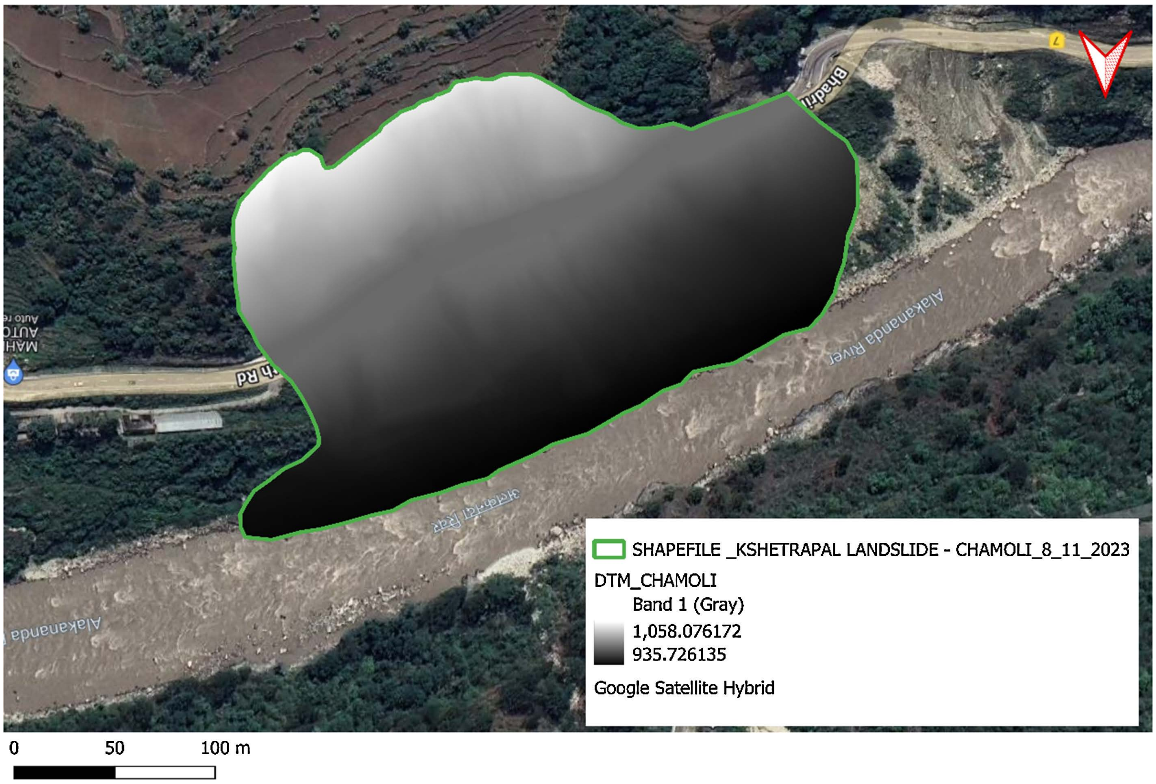

Figure 8. Showing Digital Terrain Model (DTM) of landslide area.

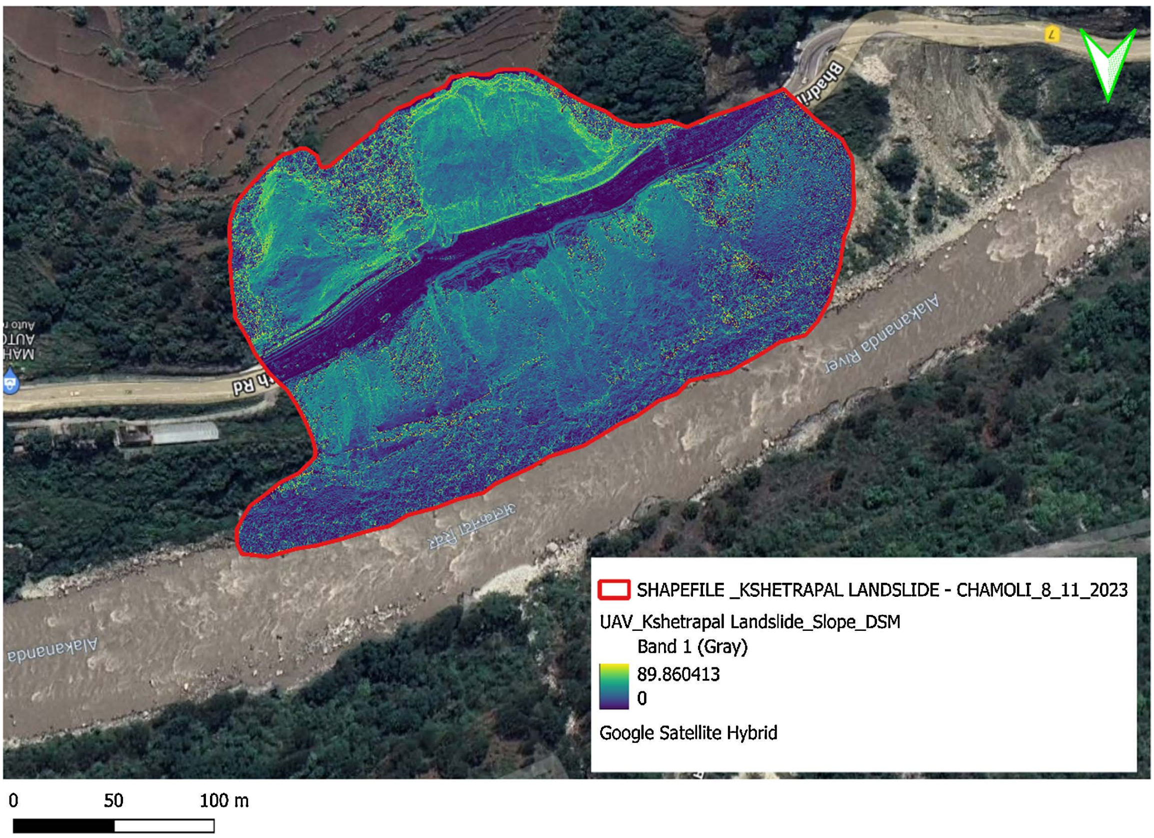

Figure 9. Showing slope of Digital Surface Model (DSM) of landslide area.

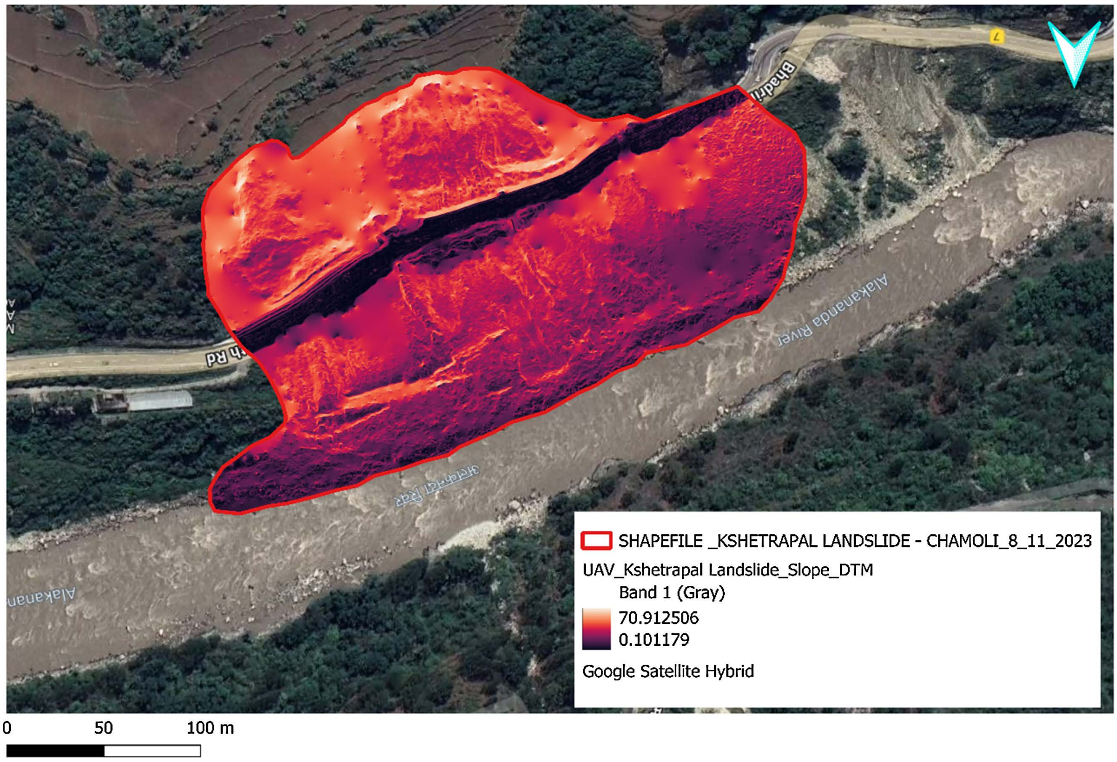

Figure 10. Showing slope of Digital Terrain Model (DTM) of landslide area.

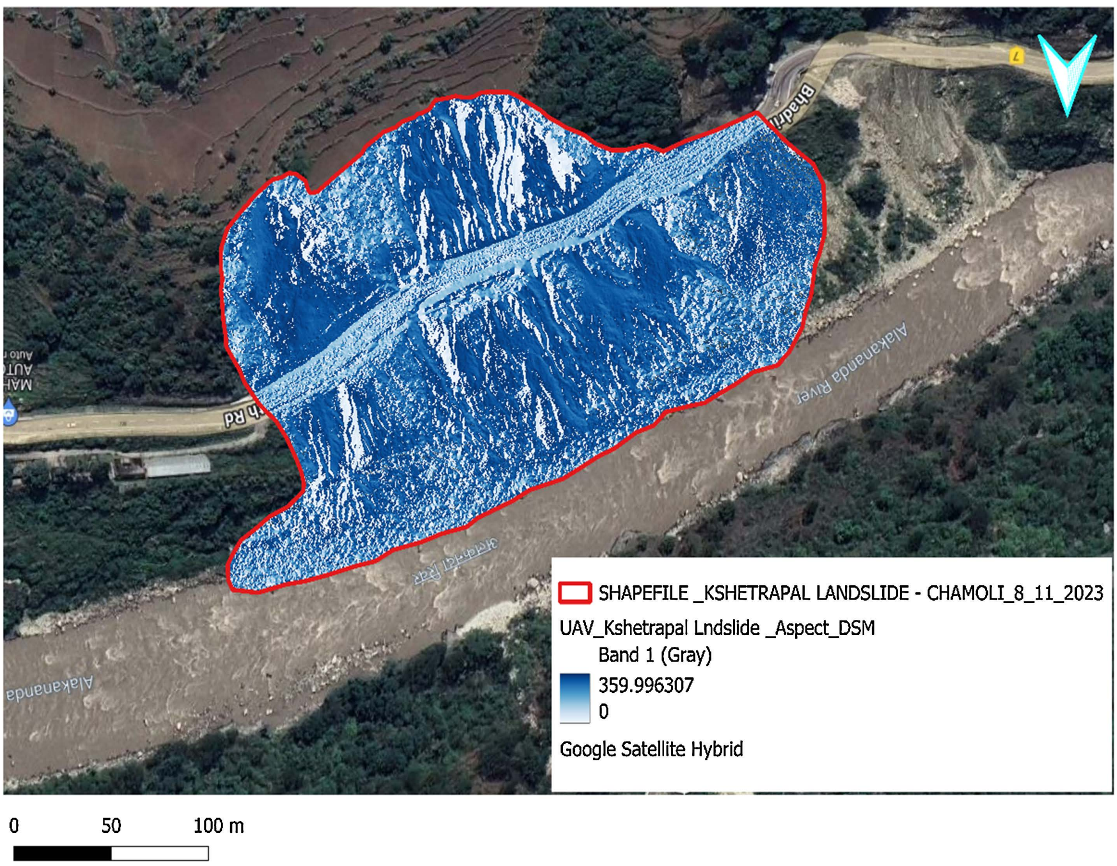

Figure 11. Showing aspect of Digital Surface Model (DSM) of landslide area.

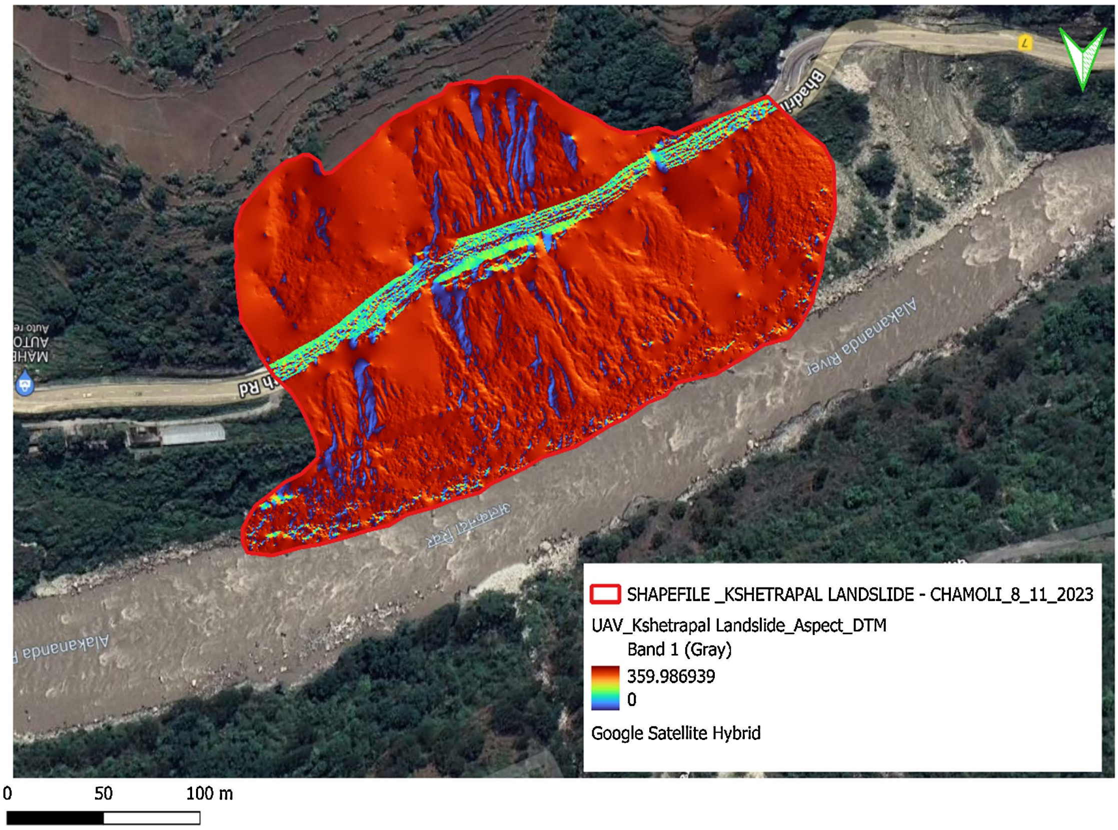

Figure 12. Showing aspect of Digital Terrain Model (DTM) of landslide area.

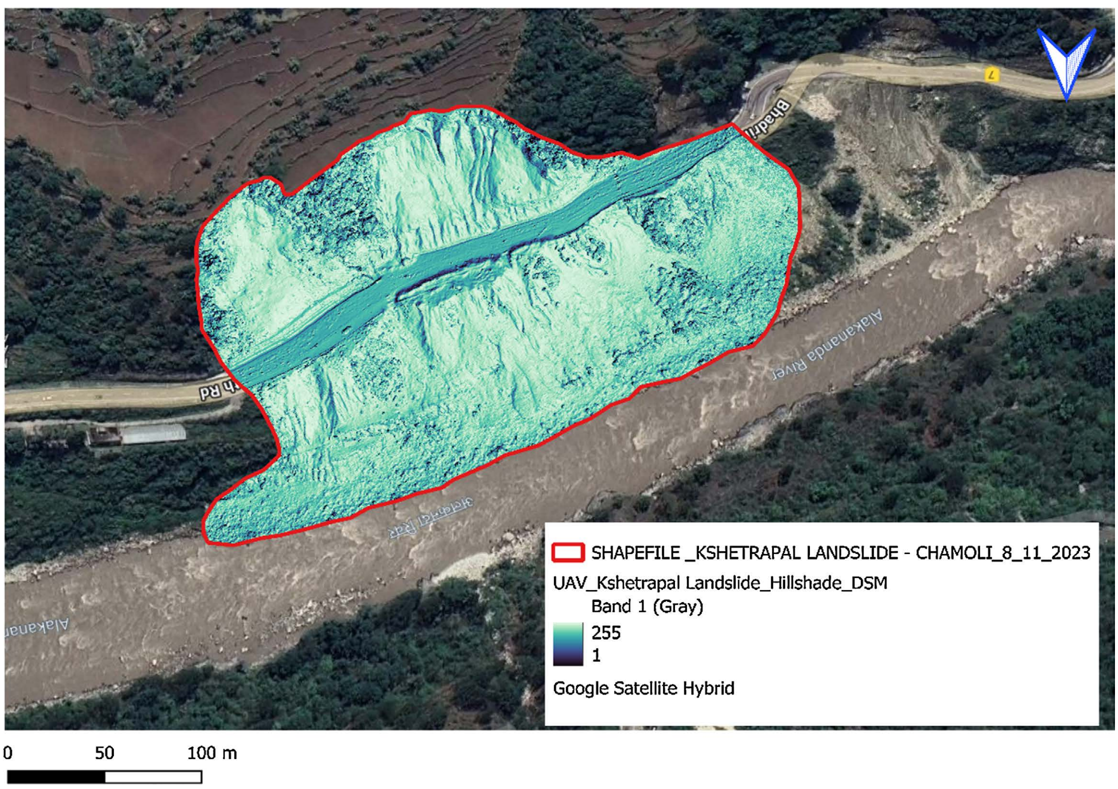

Figure 13. Showing hillshade of Digital Surface Model (DSM) of landslide area.

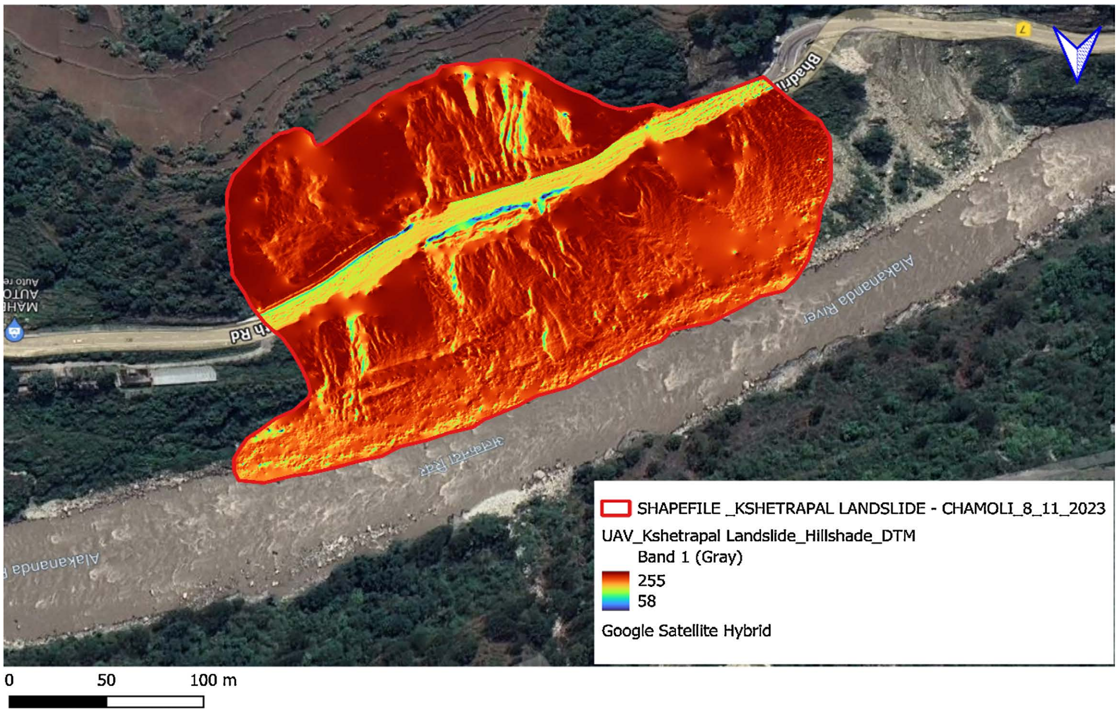

Figure 14. Showing hillshade of Digital Terrain Model (DTM) of landslide area.

3. Study Area

Kshetrapal Landslide, Chamoli district in Uttarakhand state. Its latitude and longitude range between 29˚50'N to 30˚40'N and 78˚40'E to 79˚50'E. The area is highly prone to frequent hazards like landslides.

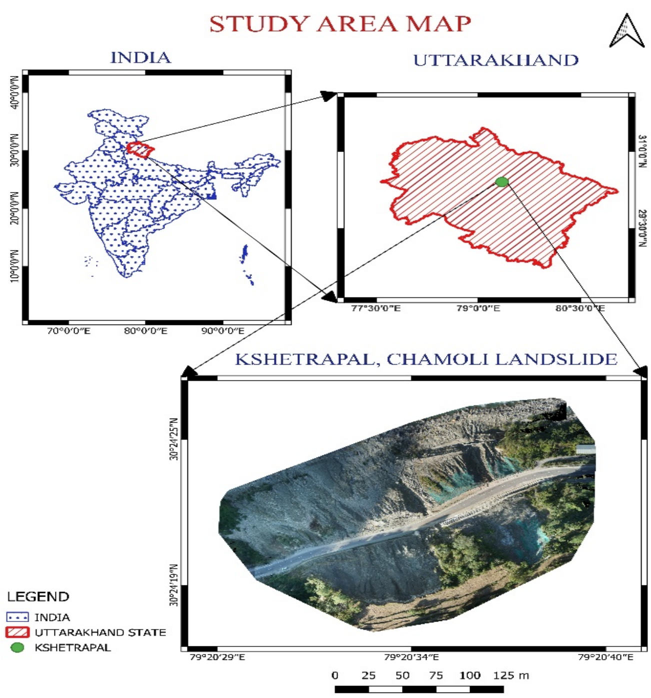

(a)

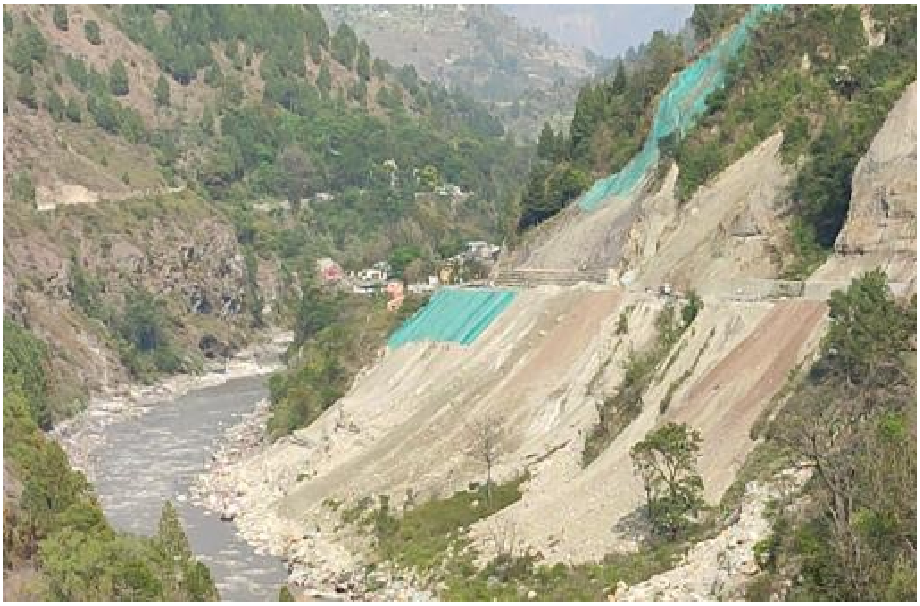

(b)

Figure 15. (a) Study area of landslide and (b) Kshetrapal landslide, Chamoli district in Uttarakhand.

Chamoli district, the second largest district of Uttarakhand, is also important from a strategic point of view as it shares its northern boundary with Tibet (China). District Chamoli shares its north-western boundary with Uttarkashi, the western boundary with Rudraprayag district, the south-western boundary with Tehri Garhwal district, the southern boundary with Almora district, the south-eastern boundary with Baleshwar district and eastern & north-eastern boundary with Pithoragarh district

4. Data Acquisition and Processing

4.1. Data Acquisition

For collecting data of Kshetrapal landslide area, Chamoli-District, Uttarakhand, India, TLS and UAV was used (**Figure 16**). TLS is a type of remote detecting that employs lasers to gather 3D spatial data from environmental study targets.

TLS has strong penetration in vegetated areas, high accuracy, and strong stability. UAV mapping creates 2D aerial data and produces 3D clouds of point photos as opposed to TLS. Its field of vision is less constrained by the terrain; thus, it can gather more topographical data in a shorter amount of time. Aerial triangulation, a technique for tying point densification that makes use of the inherent geometric properties of aerial photogrammetry, produces the 3D clouds of points of UAV mapping. A local organization model (optical or computerized) that corresponds to the arena is built using overlapped aerial photos and photogrammetric techniques, and densified point cloud sets are given planar coordinates and elevations using this method. UAV aerial photography typically has better accuracy and resolution than TLS.

(a)

(b)

Figure 16. On-site surveys through TLS and UAV. (a) On-site data collection for TLS; (b) On-location UAV aeronautical photograph.

4.1.1. Data Collection by UAV

1) Mission Planning:

- Autonomous flights are executed using the UAV.
- Prior to flight, comprehensive mission planning is conducted utilizing CD fly software.
- Essential parameters such as side and front overlap percentages, flight altitude, takeoff altitude, and flight speed are carefully defined as inputs for the flight plan.
- Flight plans can be established by:
  - Importing a .kml file containing the desired survey area.
  - Manually drawing the survey area on the Google Satellite base map within the software interface.

2) Data Capture:

- The UAV is set to autonomous flight mode to capture images.
- The UAV maintains a consistent flight height of 120 meters throughout the mission, effectively capturing the terrain.
- The survey plan is imported from Google Earth Pro to visualize the flight path in 3D terrain before commencing the flight.

- The UAV's onboard GPS continuously logs latitude, longitude, and altitude information at each waypoint defined within the mission plan.

3) PPK Data Processing and Geotagging:

- The GPS data collected by the base station and the rover (UAV) is processed using the open-source "rtklib" library.
- The "rtkconv" library is employed to convert the raw GPS data into the RINEX format.
- Subsequently, "rtkpost" is utilized for post-processing kinematics, refining the GPS data for accurate positioning.
- The raw images captured by the UAV are geotagged using the Geotag PPK software, incorporating the processed base and rover data.

4) Data Processing and Product Generation:

- The geotagged images are processed using Pix4Dmapper software.
- The software leverages Structure-from-Motion (SfM) algorithms to:
  - Extract matching features between images.
  - Generate a 3D surface geometry (point cloud).
  - Create an orthophoto map.
  - Produce a high-resolution digital elevation model (DEM).

4.1.2. Data Collection by TLS

1) Target Placement:

- Strategically place checkerboards and spherical targets on the landslide face in close proximity to the TLS instrument.
- Consider placing targets in the immediate vicinity or directly in front of the scanning area.

2) TLS Stationing:

- Establish TLS stations at intervals of 10 - 15 meters along the length of the landslide. This ensures adequate coverage and overlap between scans.

3) Data Acquisition:

- Conduct TLS scans at each station for approximately 10 minutes.
- Utilize 1/4th image quality settings to balance data acquisition speed and resolution.
- During each scan, ensure that the previous scan's targets remain within the field of view of the current scan. This facilitates accurate alignment and registration of the point clouds.

4) Data Collection:

- Acquire TLS scans along with corresponding RGB images.
- This combined data allows for the generation of a visually rich and informative colored point cloud of the landslide face, enhancing the analysis and interpretation of the landslide features.

4.2. Image Processing

The observational evidence shows that UAV technology can be used to exhibit a comprehensive surveillance strategy in ground measuring engaged in collapse.

The current study's surface observation method and data image analysis flowchart are shown in **Figure 17**. Photogrammetric programs are used to collect research site data and analyze images. Data analysis begins after data collection. The 3D model was georeferenced utilizing determined control points after processing the data. DEM would be developed here.

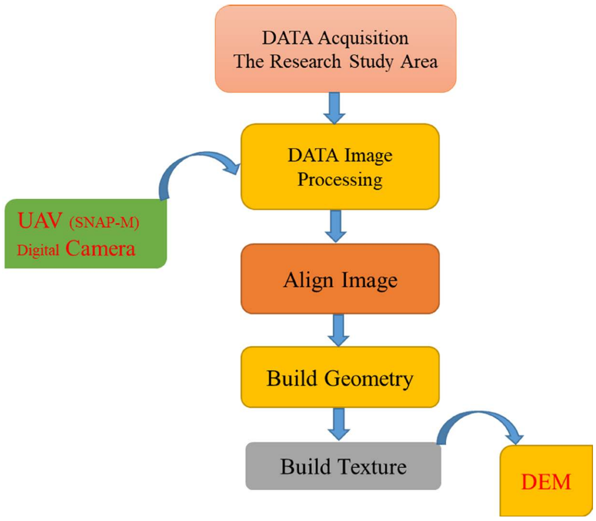

Figure 17. Flowchart of UAV.

4.3. SEVEN DEMs

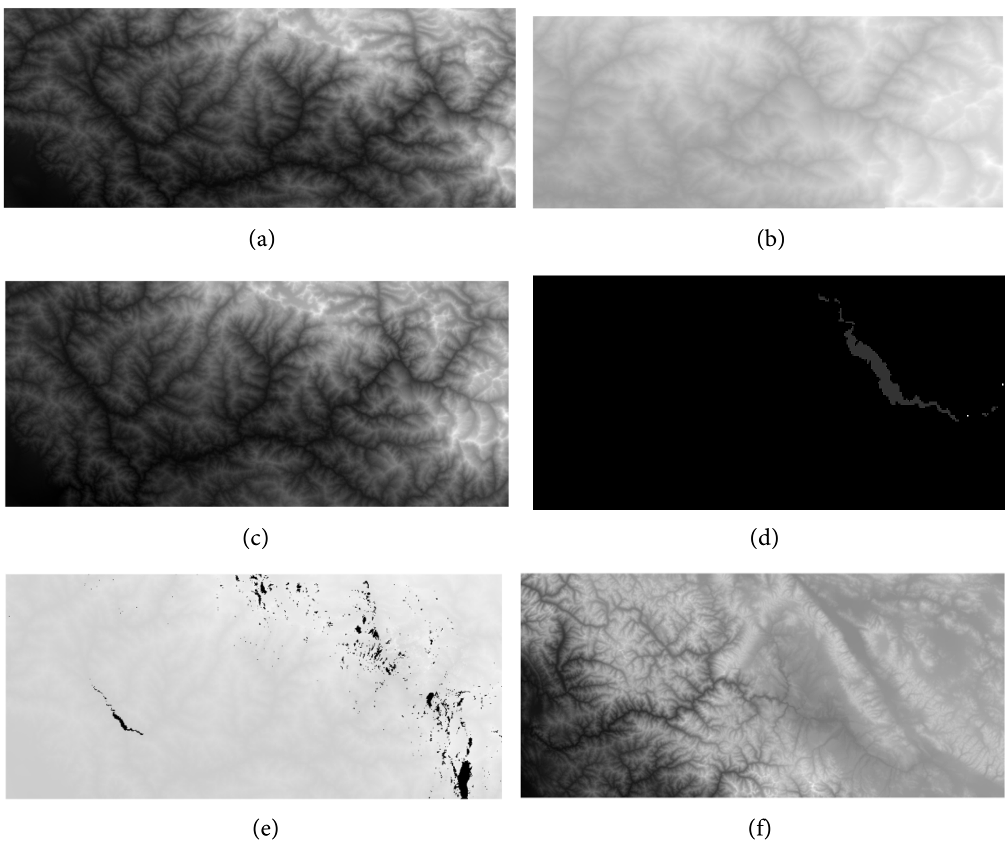

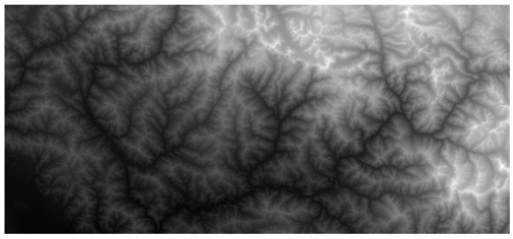

(g)

Figure 18. Showing various DEMs. (a) Cartosat DEM; (b) ASTER DEM; (c) SRTM DEM; (d) Alos 3D DEM; (e) TanDEM DEM; (f) MERIT DEM; (g) Fathom DEM.

4.3.1. CARTOSAT

A High-resolution Digital Elevation Model (CartoDEM) was created by the Indian Space Research Organization (ISRO) with data from the Cartosat-1 satellite. Among the many uses for CartoDEM's precise surface elevation data are topographic mapping, city planning, infrastructure construction, watershed management, and catastrophe prevention and mitigation. With a spatial resolution of around 30 meters, it is well-suited for mapping and analyzing large-scale areas. For initiatives in India's public and commercial sectors that need accurate terrain data, CartoDEM is a must-have geospatial analytic tool. **Figure 18(a)** (Source: https://www.isro.gov.in/Cartosat_1_Completes_a_Decade_in_orbit.html)

4.3.2. ASTER

NASA's Terra Satellite's Advanced Space Borne Thermal Emission and Reflection Radiometer (ASTER) sensor acquired worldwide elevation data to create the ASTER Digital Elevation Model (DEM). ASTER DEM, launched in 1999, offers 30-meter elevation data for most of Earth between latitudes 83˚N and 83˚S. This DEM is utilized in topographic mapping, climate modeling, land-use planning, and natural hazard assessment. High-resolution elevation data permits extensive topography study, making it useful for academics and planners worldwide. **Figure 18(b)** (Source: https://asterweb.jpl.nasa.gov/gdem.asp)

4.3.3. SRTM

NASA and the National Geospatial-Intelligence Agency (NGA) developed the Shuttle Radar Topography Mission (SRTM) Digital Elevation Model (DEM) in 2000, which provides comprehensive elevation information on a worldwide scale. SRTM used radar interferometry to collect elevation data with almost worldwide coverage between latitudes 60˚N and 56˚S, with a resolution of 30 meters in the United States and 90 meters in the majority of other areas. This DEM is widely used in hydrology, geology, environmental management, and urban planning. It aids in terrain analysis, flood modeling, and infrastructure development by providing accessible and reliable elevation data for a broad range of applications throughout the globe. **Figure 18(c)** (Source: https://www.earthdata.nasa.gov/sensors/srtm)

4.3.4. ALOS 3D

The Advanced Land Observing Satellite (ALOS) 3D, commonly known as ALOS

World 3D (AW3D), is a high-resolution global digital elevation model (DEM) created from data collected by the Panchromatic Remote-sensing Instrument for Stereo Mapping (PRISM) aboard Japan's ALOS satellite. The ALOS 3D DEM has a spatial resolution of up to 5 meters, making it one of the most precise global elevation models currently accessible. It covers the whole terrestrial area of the Earth and is used in a variety of applications such as disaster management, urban planning, infrastructure construction, and environmental monitoring. Its great precision and rich detail make it an indispensable tool for detailed terrain research and geospatial investigations. **Figure 18(d)** (Source: https://earth.esa.int/eogateway/missions/alos)

4.3.5. TanDEM

TanDEM is Designed by the German Aerospace Center (DLR) in collaboration with Airbus Defence and Space, TanDEM is a digital elevation model (DEM). Two very similar satellites, TerraSAR and TanDEM, flying in close formation to provide an extremely precise, worldwide DEM, comprised this project. With vertical accuracy between 1 and 2 meters, the TanDEM DEM offers elevation data at a 12-meter spatial resolution. Widely utilized for purposes in topographic mapping, hydrology, forestry, infrastructure development, and disaster management, it covers the whole terrestrial surface of the Earth. For thorough terrain study and many scientific and commercial tasks, the exact elevation data from TanDEM is indispensable. **Figure 18(e)** (Source: https://gdk.gdi-de.org/geonetwork/srv/api/records/5eecdf4c-de57-4624-99e9-60086b032aea).

4.3.6. MERIT

MERIT DEM, which stands for "Multi-Error-Removed Improved-Terrain DEM," is a global digital elevation model that makes earlier DEM datasets, like SRTM and ASTER, more accurate by getting rid of many of the mistakes they had. MERIT DEM was created by experts at the University of Tokyo and other schools working together. It fixes mistakes such as absolute bias, stripe noise, tree height bias, and more. It gives a good elevation model with a precision of about 3 seconds, which is about 90 meters at the equator. This makes it useful for water modeling, figuring out the risk of flooding, and other earth science tasks. The best thing about MERIT DEM is that it is more accurate and consistent, which makes it easier to do more accurate and in-depth analyses in many geospatial studies. **Figure 18(f)** (Source: http://hydro.iis.u-tokyo.ac.jp/~yamadai/MERIT_DEM/)

4.3.7. FABDEM

Forest and Buildings Gone Copernicus DEM is a modified DEM. FABDEM removes forest canopies and structures from regular DEMs to better portray the naked soil. Hydrological modeling, flood risk assessment, and infrastructure design benefit from an unobstructed perspective of the terrain. FABDEM uses vegetation and structural correction methods to provide a dataset that better depicts land topography. **Figure 18(g)** (Source: https://gee-community-catalog.org/projects/fabde)

4.4. Morphometric Analysis of "White Box Tool" (WBT)

White Box Tool (WBT) is plugging-in software specifically designed to study geographical data. It includes a comprehensive collection of more than 550 tools designed for the manipulation and analysis of various forms of geographical data. One of its notable attributes is its wide utilization of parallel computing, eliminating the requirement for additional libraries like GDAL. The white box approach utilizes prior knowledge of geometry to formulate its model.

The WBT enables detailed morphometric evaluation of terrain features that are important for studying landslides in the Chamoli district of the Himalayas. By utilizing high-resolution DEMs obtained from UAV or TLS data, researchers are able to calculate important factors such as slope angle, topographic indices and aspect using the following mathematical formulas:

$$\text{Slope degree} = \arctan\left(\sqrt{\left(\frac{\partial w}{\partial u}\right)^2 + \left(\frac{\partial w}{\partial v}\right)^2}\right) \tag{1}$$

The symbols $\frac{\partial w}{\partial u}$ and $\frac{\partial w}{\partial v}$ represent the fractional derivatives of the elevation w with respect to the variables u and v, accordingly.

$$\text{Aspect (degree)} = \text{arctan2}\left(-\frac{\partial w}{\partial v}, -\frac{\partial w}{\partial u}\right) + 360^\circ \text{ (if less than 0)} \tag{2}$$

The arctan2 function is a mathematical function that calculates an angle from the coordinates u and v of the Cartesian plane.

$$\text{Topographic Wetness Index (TWI)} = \ln\left(\frac{A}{\tan(\beta)}\right) \tag{3}$$

where A is the local upslope contributing area and β is the local slope gradient in radians.

$$\text{Compound Topographic Index (CTI)} = \ln\left(\frac{A}{\tan(\beta)}\right) \times S\text{, where S is the slope.} \tag{4}$$

These formulas illustrate how Whitebox Tool utilizes mathematical expressions to compute various morphometric parameters essential for terrain analysis and modeling. The software automates these calculations based on input DEM data, providing researchers with quantitative insights into landscape characteristics and processes. These metrics provide insights into terrain stability and susceptibility to landslides. White box method interprets the DEM geometry directly into UAV parameters using a compilation of formulae software such as DATCOM, AVL or TORNADO. By leveraging advanced geospatial techniques, this software supports informed decision-making for disaster risk reduction and land management strategies in Chamoli and similar Himalayan environments. In the context of landslide research, White Box Tool serves as a versatile toolset for morphometric analysis, offering capabilities to derive detailed terrain parameters essential for assessing landslide risk factors and identifying vulnerable areas.

5. Comparing QGIS and WBT Values of Various DEMs

Comparison (differences in values) of seven (7) different DEMs between two algorithms used, *i.e.*, QGIS, White Box Tool (WBT), were successfully attempted in the present research. The TLS data, UAV data, and Satellite data of the study area were subjected to two different algorithms (QGIS and WBT) to evaluate and differentiate seven different DEMs (CARTOSAT, ASTER, SRTM, Alos 3D, TanDEM, MERIT, and FabDEM/FATHOM) taking into consideration various parameters viz. Aspect, Hillshade, Slope, Mean Curvature, Plan Curvature, Profile Curvature and Total Curvature. The different values of aforesaid parameters of various DEMs evaluated reveal that only three parameters, *i.e.*, Aspect, Hillshade, and Slope, show results. In contrast, the remaining ones do not show any meaningful results, and therefore, the comparison was possible only with regard to these three parameters. The comparison is drawn by comparing minimum, maximum, and elevation values (by subtracting WBT values from QGIS values) regarding Aspect, Hillshade, and Slope, arranging the differences in values as per their importance. (increasing or decreasing order), assigning merit scores individually, and then cumulatively, and ascertaining the order of application suitability of various DEMs, which stand in the order of (CARTOSAT, ASTER, SRTM, ALOS 3D, TanDEM, and MERIT, and FabDEM/FATHOM). (Refer to Tables 1-12)

Table 1. Cartosat DEM's comparison between QGIS and WBT parameters.

S.No.	QGIS DEM's	WBT DEM's	Name of Parameters
1.			Slope
2.			Aspect
3.	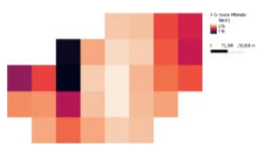	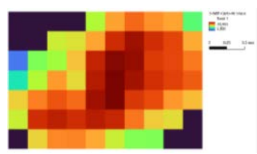	Hillshade

Table 2. ASTER DEM's comparison between QGIS and WBT parameters.

S.No.	QGIS DEM's	WBT DEM's	Name of Parameters
1.	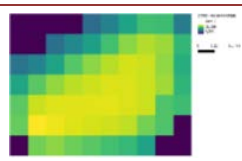	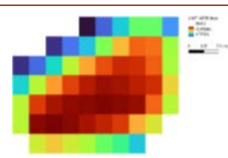	Slope

Continued

2.			Aspect
3.			Hillshade

Table 3. SRTM DEM's com comparison pare between QGIS and WBT parameters.

S.No.	QGIS DEM's	WBT DEM's	Name of Parameters
1.	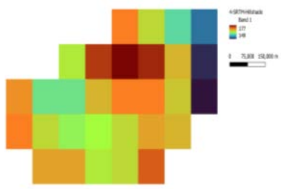	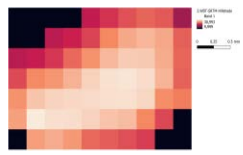	Slope
2.		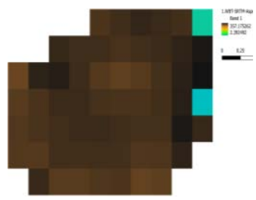	Aspect
3.			Hillshade

Table 4. Alos 3D DEMs comparison between QGIS and WBT parameters.

S.No.	QGIS DEM's	WBT DEM's	Name of Parameters
1.		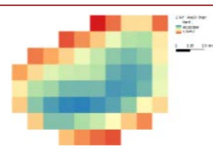	Slope
2.			Aspect
3.		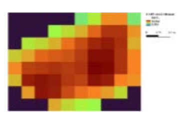	Hillshade

Table 5. TanDEM DEMs comparison between QGIS and WBT parameters.

S.No.	QGIS DEM's	WBT DEM's	Name of Parameters
1.	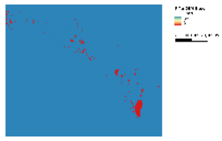		Slope
2.	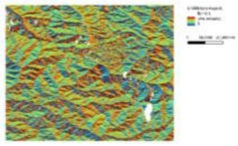	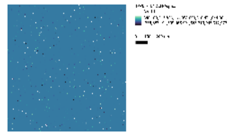	Aspect
3.	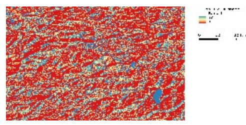	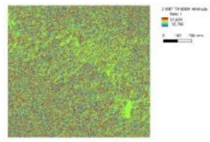	Hillshade

Table 6. MERIT DEMs comparison between QGIS and WBT parameters.

S.No.	QGIS DEM's	WBT DEM's	Name of Parameters
1.	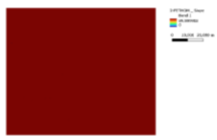		Slope
2.	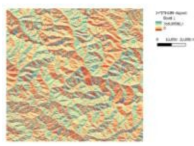	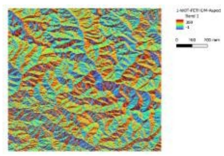	Aspect
3.	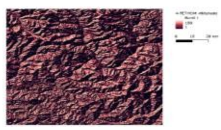	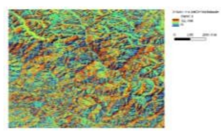	Hillshade

Table 7. FabDEM/Fathom DEM's comparison between QGIS and WBT parameters.

S.No.	QGIS DEM's	WBT DEM's	Name of Parameters
1.	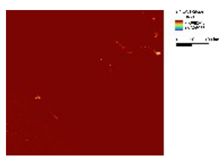	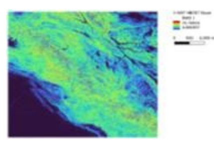	Slope
2.	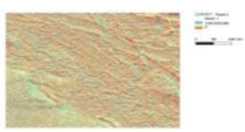		Aspect
3.	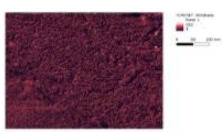	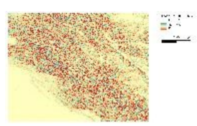	Hillshade

Table 8. Kshetrapal landslides, Chamoli (area wise)—data analysis from QGIS.

S. No.	Name of Landslides	DEM's	Slope			Aspect			Hillshade		
			Range of Values			Range of Values			Range of Values		
			Minimum	Maximum	Elevation	Minimum	Maximum	Elevation	Minimum	Maximum	Elevation
1.	Kshetrapal Landslide, Chamoli	CartoSat 30 m	89.998077	89.999397	20 mm	4.166504	354.80557	20 mm	116	179	150,000 mm
2.		ASTER 30 m	89.998489	89.999382	20 mm	334.01077	347.54175	20 mm	152	171	200 km
3.		SRTM 30 m	89.998543	98.999527	50 mm	325.8403	349.39615	20 m	149	177	150,000 m
4.		Alos 3D 30 m	89.998932	89.999451	20 m	323.82037	349.3078	50 m	149	178	150 Km
5.		TanDEM 90 m	0	90	20,000 m	0	359.99365	20,000 m	1	181	20 km
6.		Merit 90 m	16.328936	89.999809	100 km	0	359.99927	100 km	1	252	100 km
7.		Pathom/ FABDEM 30 m	0	89.999908	20,000 m	0	359.99982	20,000 m	1	188	20 km

Table 9. Kshetrapal landslides, Chamoli (area wise)—data analysis from WBT.

S. No.	Name of Landslides	DEM's	Slope			Aspect			Hillshade		
			Range of Values			Range of Values			Range of Values		
			Minimum	Maximum	Elevation	Minimum	Maximum	Elevation	Minimum	Maximum	Elevation
1.	Kshetrapal Landslide, Chamoli	CartoSat 30 m	6.79865	41.300053	0.5 mm	2.075129	357.58582	0.5 mm	9999	30,983	0.5mm
2.		ASTER 30 m	1.707192	40.470341	0.5 mm	13.489829	359.99991	0.5 mm	9999	30,584	0.5 mm
3.		SRTM 30 m	6.717078	47.17078	0.5 mm	2.392492	357.17526	0.5 mm	9999	30,993	0.5 mm
4.		Alos 3D 30 m	4.90452	43.253864	0.5 mm	13.8176	352.07877	0.5 mm	9999	30,860	0.5 mm
5.		TanDEM 90 m	−3,39,883	3,39,079	150 mm	−336,867	340,008	200 mm	−32,766	32,639	200 mm
6.		Merit 90 m	0.000157	71.76545	1000 mm	−1	360	1000 mm	0	32,756	1000 mm
7.		Pathom/ FABDEM 30 m	0	81.011169	200 mm	−1	360	200 mm	0	32,766	200 mm

Table 10. Slope results of DEMs.

S.No.	DEM's	QGIS			WBT			Differences Values		
		Minimum	Maximum	Elevation	Minimum	Maximum	Elevation	Minimum	Maximum	Elevation
1.	CartoSat 30 m	89.998077	89.999397	20 mm	6.79865	41.30005	0.5 mm	83.19943	48.69934	19.5
2.	ASTER 30 m	89.998489	89.999382	20 mm	1.707192	40.47034	0.5 mm	88.2913	49.52904	19.5
3.	SRTM 30 m	89.998543	98.999527	50 mm	6.717078	47.17078	0.5 mm	83.28147	51.82875	49.5
4.	Alos 3D 30 m	89.998932	89.999451	20 m	4.90452	43.25386	0.5 mm	85.09441	46.74559	19,999.5
5.	TanDEM 90 m	0	90	20,000 m	−339,883	339,079	150 mm	339883	−338989	19,999,850
6.	Merit 90 m	16.328936	89.999809	100 km	0.000157	71.76545	1000 mm	16.32878	18.23436	99,999,000
7.	Pathom/ FABDEM 30 m	0	89.999908	20,000 m	0	81.01117	200 mm	0	8.988739	19,999,800

Table 11. ASPECT results of DEMs.

		QGIS			WBT			Differences Values		
S.No.	DEM's	Minimum	Maximum	Elevation	Minimum	Maximum	Elevation	Minimum	Maximum	Elevation
1.	CartoSat 30 m	4.166504	354.805572	20 mm	2.075129	357.5858	0.5 mm	2.091375	−2.78024	19.5
2.	ASTER 30 m	334.010773	347.541748	20 mm	13.48983	359.9999	0.5 mm	320.5209	−12.4582	19.5
3.	SRTM 30 m	325.840302	349.396149	20 m	2.392492	357.1753	0.5 mm	323.4478	−7.77911	19999.5
4.	Alos 3D 30 m	323.820374	349.3078	50 m	13.8176	352.0788	0.5 mm	310.0028	−2.77097	49999.5
5.	TanDEM 90 m	0	359.993652	20,000 m	−336,867	340,008	200 mm	336,867	−339648	19,999,800
6.	Merit 90 m	0	359.999268	100 km	−1	360	1000 mm	1	−0.00073	99,999,000
7.	Pathom/ FABDEM 30 m	0	359.999817	20,000 m	−1	360			−0.00018	19,999,800

Table 12. Hillshade results of DEMs.

		QGIS			WBT			Differences Values		
S.No.	DEM's	Minimum	Maximum	Elevation	Minimum	Maximum	Elevation	Minimum	Maximum	Elevation
1.	CartoSat 30 m	116	179	150,000 mm	9999	30,983	0.5mm	−9883	−30,804	150,000
2.	ASTER 30 m	152	171	200 km	9999	30,584	0.5 mm	−9847	−30,413	200,000,000
3.	SRTM 30 m	149	177	150,000 m	9999	30,993	0.5 mm	−9850	−30,816	150,000,000
4.	Alos 3D 30 m	149	178	150 Km	9999	30,860	0.5 mm	−9850	−30,682	150,000,000
5.	TanDEM 90 m	1	181	20 km	−32,766	32,639	200 mm	32,767	−32,458	19,999,800
6.	Merit 90 m	1	252	100 km	0	32,756	1000 mm	1	−32,504	99,999,000
7.	Pathom/ FABDEM 30 m	1	188	20 km	0	32,766	200 mm	1	−32,578	19,999,800

6. Comparison of Application Suitability of Various Dems

For concluding suitability of various DEMs, differences in Minimum values, Maximum values and Elevation values were arranged in increasing/decreasing order and assigned merit score with reference to Slope (Table 13(a)-(c)), Aspect (Table 14(a)-(c)), and Hillshade (Table 15(a)-(c)).

7. Cumulative Merit Scores of Slope, Aspect, and Hillshade vs Preferred Application of Various DEMs

Merit of Application of DEMs with reference to Slope, Aspect and Hillshade (Refer Tables 16-18).

From Table 19 below, it is evident that for Minimum, Maximum and Elevation Values of Slope, the cumulative merit score is 21+, 19+, 16+, 13+, 10+, 7+ and 5+ and accordingly, the preferred DEM's will be in the same order *i.e.* CartoSat 30 m, ASTER 30 m, SRTM 30 m, Alos 3D 30 m, Merit 90 m and Fathom/FabDEM 30 m.

Table 13. (a) Comparison of applicability/suitability of various DEM's w.r.t slope minimum values; (b) Comparison of applicability/suitability of various DEM's w.r.t slope maximum values; (c) Comparison of applicability/suitability of various DEM's w.r.t slope elevation values.

(a)

S.No.	DEM's	Difference in Minimum Values	Arranged in Increasing Order	Merit Score
1	CartoSat 30 m	83.19943	0	7+
2	ASTER 30 m	88.2913	16.32898	6+
3	SRTM 30 m	83.28147	83.19943	5+
4	Alos 3D 30 m	85.09441	83.28147	4+
5	TanDEM 90 m	339883	85.09441	3+
6	Merit 90 m	16.32898	88.2913	2+
7	Fathom/FABDEM 30 m	0	339883	1+

(b)

S.No.	DEM's	Difference in Maximum Values	Arranged in Decreasing Order	Merit
1	CartoSat 30 m	48.69934	51.82875	7+
2	ASTER 30 m	49.52904	49.52904	6+
3	SRTM 30 m	51.82875	48.69934	5+
4	Alos 3D 30 m	46.74559	46.74559	4+
5	TanDEM 90 m	−338989	18.23436	3+
6	Merit 90 m	18.23436	8.988739	2+
7	Fathom/FABDEM 30 m	8.988739	8.988739	2+

(c)

S.No.	DEM's	Difference in Elevation Values	Arranged in Increasing Order	Merit
1	CartoSat 30 m	19.5	19.5	7+
2	ASTER 30 m	19.5	19.5	7+
3	SRTM 30 m	49.5	49.5	6+
4	Alos 3D 30 m	19999.5	19999.5	5+
5	TanDEM 90 m	19999850	19999800	4+
6	Merit 90 m	99999000	19999850	3+
7	Fathom/FABDEM 30 m	19999800	99999000	2+

Table 14. (a) Comparison of applicability/suitability of various DEM's w.r.t aspect minimum values; (b) Comparison of applicability/suitability of various DEM's w.r.t aspect maximum values; (c) Comparison of applicability/suitability of various DEM's w.r.t aspect elevation values.

(a)

S.No.	DEM's	Difference in Minimum Values	Arranged in Increasing Order	Merit Score
1	CartoSat 30 m	2.091375	1	7+
2	ASTER 30 m	320.5209	1	7+
3	SRTM 30 m	323.4478	2.091375	6+
4	Alos 3D 30 m	310.0028	310.0028	5+
5	TanDEM 90 m	336867	320.5209	4+
6	Merit 90 m	1	323.4478	3+
7	Fathom/FABDEM 30 m	1	336867	2+

(b)

S.No.	DEM's	Difference in Maximum Values	Arranged in Decreasing Order	Merit
1	CartoSat 30 m	−2.7804	−0.00018	7+
2	ASTER 30 m	−12.4582	−0.00073	6+
3	SRTM 30 m	−7.77911	−2.77097	5+
4	Alos 3D 30 m	−2.77097	−2.7804	4+
5	TanDEM 90 m	−339648	−7.77911	3+
6	Merit 90 m	−0.00073	−12.4582	2+
7	Fathom/FABDEM 30 m	−0.00018	−339648	1+

(c)

S.No.	DEM's	Difference in Elevation Values	Arranged in Increasing Order	Merit
1	CartoSat 30 m	19.5	19.5	7+
2	ASTER 30 m	19.5	19.5	7+
3	SRTM 30 m	19,999.5	19,999.5	6+
4	Alos 3D 30 m	49,999.5	49,999.5	5+
5	TanDEM 90 m	19,999,800	19,999,800	4+
6	Merit 90 m	99,999,000	19,999,800	4+
7	Fathom/FABDEM 30 m	19,999,800	99,999,000	3+

Table 15. (a) Comparison of applicability/suitability of various DEM's w.r.t hillshade minimum values; (b) Comparison of applicability/suitability of various DEM's w.r.t hillshade maximum values; (c) Comparison of applicability/suitability of various DEM's w.r.t hillshade elevation values.

(a)

S.No.	DEM's	Difference in Minimum Values	Arranged in Increasing Order	Merit Score
1	CartoSat 30 m	−9883	−9883	7+
2	ASTER 30 m	−9847	−9850	6+
3	SRTM 30 m	−9850	−9850	6+
4	Alos 3D 30 m	−9850	−9847	5+
5	TanDEM 90 m	32,767	1	4+
6	Merit 90 m	1	1	4+
7	Fathom/FABDEM 30 m	1	32,767	3+

(b)

S.No.	DEM's	Difference in Maximum Values	Arranged in Decreasing Order	Merit
1	CartoSat 30 m	−30,804	−30,413	7+
2	ASTER 30 m	−30,413	−30,682	6+
3	SRTM 30 m	−30,816	−30,804	5+
4	Alos 3D 30 m	−30,682	−30,816	4+
5	TanDEM 90 m	−32,458	−32,458	3+
6	Merit 90 m	−32,504	−32,504	2+
7	Fathom/FABDEM 30 m	−32,578	−32,578	1+

(c)

S.No.	DEM's	Difference in Elevation Values	Arranged in Increasing Order	Merit
1	CartoSat 30 m	15,000	15,000	7+
2	ASTER 30 m	200,000,000	19,999,800	6+
3	SRTM 30 m	150,000,000	19,999,800	6+
4	Alos 3D 30 m	150,000,000	99,999,800	5+
5	TanDEM 90 m	19,999,800	150,000,000	4+
6	Merit 90 m	99,999,800	150,000,000	4+
7	Fathom/FABDEM 30 m	19,999,800	200,000,000	3+

Table 16. Merit of application of DEMs with reference to slope.

S.No.	Difference in Minimum Value Merit Score	Difference in Maximum Merit Score	Difference in Elevation Value Merit Score	Cumulative Score Merit Score	Preferred DEM's Merit Score
1	7+	7+	7+	21+	CartoSat 30 m
2	6+	6+	7+	19+	ASTER 30 m
3	5+	5+	6+	16+	SRTM 30 m
4	4+	4+	5+	13+	Alos 3D 30 m
5	3+	3+	4+	10+	TanDEM 90 m
6	2+	2+	3+	7+	Merit 90 m
7	1+	2+	2+	5+	Fathom/FABDEM 30 m

Table 17. Merit of application of DEMs with reference to aspect.

S.No.	Difference in Minimum Value Merit Score	Difference in Maximum Merit Score	Difference in Elevation Value Merit Score	Cumulative Score Merit Score	Preferred DEM's Merit Score
1	7+	7+	7+	21+	CartoSat 30 m
2	7+	6+	7+	20+	ASTER 30 m
3	6+	5+	6+	17+	SRTM 30 m
4	5+	4+	5+	14+	Alos 3D 30 m
5	4+	3+	4+	11+	TanDEM 90 m
6	3+	2+	4+	9+	Merit 90 m
7	2+	1+	3+	6+	Fathom/FABDEM 30 m

Table 18. Merit of application of DEMs with reference to hillshade.

S.No.	Difference in Minimum Value Merit Score	Difference in Maximum Merit Score	Difference in Elevation Value Merit Score	Cumulative Score Merit Score	Preferred DEM's Merit Score
1	7+	7+	7+	21+	CartoSat 30 m
2	6+	6+	6+	18+	ASTER 30 m
3	6+	5+	6+	17+	SRTM 30 m
4	5+	4+	5+	14+	Alos 3D 30 m
5	4+	3+	4+	11+	TanDEM 90 m
6	4+	2+	4+	10+	Merit 90 m
7	3+	1+	3+	7+	Fathom/FABDEM 30 m

Table 19. The merit of the application of DEM about slope minimum, maximum, and elevation.

S.No.	Difference in Minimum Value Merit Score	Difference in Maximum Value Merit Score	Difference in Elevation Value Merit Score	Cumulative Score Merit Score	Preferred DEM's Merit Score
1	7+	7+	7+	21+	CartoSat 30 m
2	6+	6+	7+	19+	ASTER 30 m
3	5+	5+	6+	16+	SRTM 30 m
4	4+	4+	5+	13+	Alos 3D 30 m
5	3+	3+	4+	10+	TanDEM 90 m
6	2+	2+	3+	7+	Merit 90 m
7	1+	2+	2+	5+	Fathom/FABDEM 30 m

From **Table 20** below, it is evident that for Minimum, Maximum, and Elevation Values of ASPECT, the cumulative merit score is 21+, 20+, 17+, 14+, 11+, 9+ and 6+ and accordingly, the preferred DEMs will be in the same order, *i.e.*, CartoSat 30 m, ASTER 30 m, SRTM 30 m, Alos 3D 30 m, Merit 90 m and Fathom/FabDEM 30 m.

Table 20. The merit of the application of DEM about aspect minimum, maximum, and elevation.

S.No.	Difference in Minimum Value Merit Score	Difference in Maximum Value Merit Score	Difference in Elevation Value Merit Score	Cumulative Score Merit Score	Preferred DEM's Merit Score
1	7+	7+	7+	21+	CartoSat 30 m
2	7+	6+	7+	20+	ASTER 30 m
3	6+	5+	6+	17+	SRTM 30 m
4	5+	4+	5+	14+	Alos 3D 30 m
5	4+	3+	4+	11+	TanDEM 90 m
6	3+	2+	4+	9+	Merit 90 m
7	2+	1+	3+	6+	Pathom/FABDEM 30 m

From **Table 21** below, it is evident that for Minimum, Maximum and Elevation Values of Hillshade the cumulative merit score is 21+, 18+, 17+, 14+, 11+, 10+ and 7+ and accordingly, the preferred DEM's will be in the same order, *i.e.*, CartoSat 30 m, ASTER 30 m, SRTM 30 m, Alos 3D 30 m, Merit 90 m and Fathom/FabDEM 30 m.

Table 21. The merit of the application of DEM about hillshade minimum, maximum, and elevation.

S.No.	Difference in Minimum Value Merit Score	Difference in Maximum Value Merit Score	Difference in Elevation Value Merit Score	Cumulative Score Merit Score	Preferred DEM's Merit Score
1	7+	7+	7+	21+	CartoSat 30 m
2	6+	6+	6+	18+	ASTER 30 m
3	6+	5+	6+	17+	SRTM 30 m
4	5+	4+	5+	14+	Alos 3D 30 m
5	4+	3+	4+	11+	TanDEM 90 m
6	4+	2+	4+	10+	Merit 90 m
7	3+	1+	3+	7+	Fathom/FABDEM 30 m

8. Conclusions

Recently, using multispectral satellite images and digital elevation models (DEMs) has become the most common way to show terrain on maps. By identifying features on high-resolution satellite pictures that record spatial, temporal, spectral, and radiometric data, one can gain a new understanding of the geomorphology of a certain area. It is also possible to use a method that works with digital elevation models (DEMs) to get information about things like slopes, aspects, hillshades, curvature, contour patterns, and 3D flythrough images. More and more, unmanned aerial vehicle (UAV) drones are being used to take High-resolution digital pictures and elevation models.

These are now an important part of making full topographic models in landslide scars that are unstable and easily worn away. An effort was made to compare (differences in values) seven (7) different DEMs between two programs, QGIS and WBT. This was successful in this study. The study area was the Kshetrapal Landslide in Chamoli District, Uttarakhand State, India. TLS, UAV, and Satellite data were used in two programs, QGIS and WBT, to compare and evaluate seven different DEMs: CartoSAT, ASTER, SRTM, Alos 3D, TanDEM, MERIT, and FabDEM/FATHOM. The parameters used were Aspect, Hillshad, Slope, Mean Curvature, Plan Curvature, Profile Curvature, and Total Curvature. Using the software QIGS and WBT to look at the different values of the above parameters of different DEMs shows that only three parameters Aspect, Hillshade, and Slope—show results. The other parameters don't show any meaningful results, so comparisons could only be made with these three parameters. The comparison is made by looking at the lowest, highest, and elevation values (by subtracting WBT values from QGIS Values) with Aspect, Hillshad, and Slope, sorting the differences in values by how important they are (increasing or decreasing order), giving each difference a merit score and then adding them all up, and figuring out the best order for using different DEMs, such as CartoSat, ASTER, SRTM, Alos 3D, TanDEM, MERIT, and FabDEM/FATHOM.

Conflicts of Interest

The author declares no conflicts of interest regarding the publication of this paper.

References

[1] Razak, K.A., Straatsma, M.W., van Westen, C.J., Malet, J.-P. and de Jong, S.M. (2011) Airborne Laser Scanning of Forested Landslides Characterization: Terrain Model Quality and Visualization. *Geomorphology*, **126**, 186-200. https://doi.org/10.1016/j.geomorph.2010.11.003

[2] Peng, T., Chen, N., Mergili, M., Hou, R. and Tian, S. (2024) Preliminary Analysis of the Mechanism in the July 16, 2022 Gaojiashan Cascading Hazard: A Landslide-Induced Debris Flow in Southwest China. *Bulletin of Engineering Geology and the Environment*, **83**, Article No. 292. https://doi.org/10.1007/s10064-024-03790-y

[3] Agrawal, S., Raghavendra, S., Kumar, S. and Pande, H. (2018) Geospatial Data for the Himalayan Region: Requirements, Availability, and Challenges. In: Navalgund, R., Kumar, A. and Nandy, S., Eds., *Remote Sensing of Northwest Himalayan Ecosystems*, Springer Singapore, 471-500. https://doi.org/10.1007/978-981-13-2128-3_22

[4] Tropeano, D. and Turconi, L. (2004) Using Historical Documents for Landslide, Debris Flow and Stream Flood Prevention. Applications in Northern Italy. *Natural Hazards*, **31**, 663-679. https://doi.org/10.1023/b:nhaz.0000024897.71471.f2

[5] Miller, A., Sirguey, P., Morris, S., Bartelt, P., Cullen, N., Redpath, T., *et al.* (2022) The Impact of Terrain Model Source and Resolution on Snow Avalanche Modeling. *Natural Hazards and Earth System Sciences*, **22**, 2673-2701. https://doi.org/10.5194/nhess-22-2673-2022

[6] Samia, J., Temme, A., Bregt, A.K., Wallinga, J., Stuiver, J., Guzzetti, F., *et al.* (2018) Implementing Landslide Path Dependency in Landslide Susceptibility Modelling. *Landslides*, **15**, 2129-2144. https://doi.org/10.1007/s10346-018-1024-y

[7] Dai, F.C., Lee, C.F. and Ngai, Y.Y. (2002) Landslide Risk Assessment and Management: An Overview. *Engineering Geology*, **64**, 65-87. https://doi.org/10.1016/s0013-7952(01)00093-x

[8] Geertsema, M. and Pojar, J.J. (2007) Influence of Landslides on Biophysical Diversity—A Perspective from British Columbia. *Geomorphology*, **89**, 55-69. https://doi.org/10.1016/j.geomorph.2006.07.019

[9] Delacourt, C., Allemand, P., Berthier, E., Raucoules, D., Casson, B., Grandjean, P., *et al.* (2007) Remote-Sensing Techniques for Analysing Landslide Kinematics: A Review. *Bulletin de la Société Géologique de France*, **178**, 89-100. https://doi.org/10.2113/gssgfbull.178.2.89

[10] McKean, J. and Roering, J. (2004) Objective Landslide Detection and Surface Morphology Mapping Using High-Resolution Airborne Laser Altimetry. *Geomorphology*, **57**, 331-351. https://doi.org/10.1016/s0169-555x(03)00164-8

[11] Ventura, G., Vilardo, G., Terranova, C. and Sessa, E.B. (2011) Tracking and Evolution of Complex Active Landslides by Multi-Temporal Airborne Lidar Data: The Montaguto Landslide (Southern Italy). *Remote Sensing of Environment*, **115**, 3237-3248. https://doi.org/10.1016/j.rse.2011.07.007

[12] Glenn, N.F., Streutker, D.R., Chadwick, D.J., Thackray, G.D. and Dorsch, S.J. (2006)

Analysis of Lidar-Derived Topographic Information for Characterizing and Differentiating Landslide Morphology and Activity. *Geomorphology*, **73**, 131-148. https://doi.org/10.1016/j.geomorph.2005.07.006

[13] Lucieer, A., Jong, S.M.d. and Turner, D. (2013) Mapping Landslide Displacements Using Structure from Motion (SfM) and Image Correlation of Multi-Temporal UAV Photography. *Progress in Physical Geography: Earth and Environment*, **38**, 97-116. https://doi.org/10.1177/0309133313515293

[14] Anand, A., Padhi, A.P. and Bhardwaj, A. (2023) Landslide Susceptibility Studies in Uttarakhand Using Novel Machine Learning-Based Model. *Image and Signal Processing for Remote Sensing XXIX*, Amsterdam, 19 October 2023, Article 1273315. https://doi.org/10.1117/12.2684332

[15] Sreenivasan, G. and Jha, C.S. (2022) Geospatial Technology for Geomorphology Mapping and Its Applications. In: Jha, C.S., Pandey, A., Chowdary, V. and Singh, V., Eds., *Geospatial Technologies for Resources Planning and Management*, Springer International Publishing, 1-47. https://doi.org/10.1007/978-3-030-98981-1_1

[16] Ahmad, N., Shafique, M., Hussain, M.L., Islam, F., Tariq, A. and Soufan, W. (2024) Characterization and Geomorphic Change Detection of Landslides Using UAV Multi-Temporal Imagery in the Himalayas, Pakistan. *Land*, **13**, Article 904. https://doi.org/10.3390/land13070904

[17] Ismail, A., Ahmad Safuan, A.R., Sa'ari, R., Wahid Rasib, A., Mustaffar, M., Asnida Abdullah, R., *et al*. (2022) Application of Combined Terrestrial Laser Scanning and Unmanned Aerial Vehicle Digital Photogrammetry Method in High Rock Slope Stability Analysis: A Case Study. *Measurement*, **195**, Article 111161. https://doi.org/10.1016/j.measurement.2022.111161

[18] Teng, J., Shi, Y., Wang, H. and Wu, J. (2022) Review on the Research and Applications of TLS in Ground Surface and Constructions Deformation Monitoring. *Sensors*, **22**, Article 9179. https://doi.org/10.3390/s22239179

[19] Dhote, P.R., Thakur, P.K., Chouksey, A., Srivastav, S.K., Raghvendra, S., Rautela, P., *et al*. (2022) Synergistic Analysis of Satellite, Unmanned Aerial Vehicle, Terrestrial Laser Scanner Data and Process-Based Modelling for Understanding the Dynamics and Morphological Changes around the Snout of Gangotri Glacier, India. *Geomorphology*, **396**, Article 108005. https://doi.org/10.1016/j.geomorph.2021.108005